Synthesis of Functionalized Triblock Copolyesters Derived from Lactic Acid and Macrolactones for Bone Tissue Regeneration

A. Martínez Cutillas,* D. Sanz-Serrano, S. Oh, F. Ventura, and A. Martínez de Ilarduya*

Synthetic and functional grafts are a great alternative to conventional grafts. They can provide a physical support and the precise signaling for cells to heal damaged tissues. In this study, a novel RGD peptide end-functionalized poly(ethylene glycol)-*b*-poly(lactic acid)-*b*-poly(globalide)-*b*-poly(lactic acid)-*b*-poly(ethylene glycol) (RGD-PEG-PLA-PGl-PLA-PEG-RGD) is synthetized and used to prepare functional scaffolds. The PGl inner block is obtained by enzymatic ring-opening polymerization of globalide. The outer PLA blocks are obtained by ring-opening polymerization of both, ʟ-lactide or a racemic mixture, initiated by the α-ω-telechelic polymacrolactone. The presence of PGl inner block enhances the toughness of PLA-based scaffolds, with an increase of the elongation at break up to 300% when the longer block of PGl is used. PLA-PGl-PLA copolymer is coupled with α-ω-telechelic PEG diacids by esterification reaction. PEGylation provides hydrophilic scaffolds as the contact angle is reduced from 114° to 74.8°. That difference improves the contact between the scaffolds and the culture media. Moreover, the scaffolds are functionalized with RGD peptides at the surface significantly enhancing the adhesion and proliferation of bone marrow-derived primary mesenchymal stem cells and MC3T3-E1 cell lines in vitro. These results place this multifunctional polymer as a great candidate for the preparation of temporary grafts.

1. Introduction

The use of polymers in tissue engineering has been growing in the last decades. They emerged as an alternative to frequently limited autografts, allografts, and xenografts.[1–5]

The replication of these conventional grafts in the laboratory is a huge challenge, but there are many synthesis pathways to come up with advanced biomaterials that solve specific tissue diseases.[6,7] If they are used to produce temporary grafts or scaffolds, they need to be non-only biodegradable, but also biocompatible and resorbable.[8–10] With this purpose, many resorbable polymers such as collagen,[11] chitosan,[12] or polyesters such as poly(lactic acid) (PLA), poly(glycolic acid) (PGA), and poly(ϵ-caprolactone) (PCL) have been utilized either alone or in combination with other biomaterials delivering promising results.[13]

In particular, PLA has proven to be one of the best candidates due to its versatility. This polyester is usually synthetized by the ring-opening polymerization (ROP) of lactide.[14] As this monomer has two enantiomeric species (ʟ-lactide and ᴅ-lactide), then isotactic poly(ʟ-lactide) (PLLA) or poly(ᴅ-lactide) can be produced. Otherwise, by using a mixture of both enantiomers or the *meso* form, heterotactic poly(ᴅ,ʟ-lactide) can be prepared.[15–17] Physical properties of PLA can be modified by the control of stereoregularity. It directly influences the crystallinity, which afterward affects the hydrolytic degradation[18,19] and, to a lesser extent, the mechanical properties.[20]

PLA has been used in medical devices for tissue regeneration that are already available in the market. Biotrak (Acumed),

A. Martínez Cutillas, S. Oh
Artificial Nature S.L.
Baldiri i Reixac 10, Barcelona 08028, Spain
E-mail: a.martinez@artificialnature.com

A. Martínez Cutillas, A. Martínez de Ilarduya
Departament d'Enginyeria Química
Universitat Politècnica de Catalunya
ETSEIB
Diagonal 647, Barcelona 08028, Spain
E-mail: antxon.martinez.de.ilarduia@upc.edu

D. Sanz-Serrano, F. Ventura
Departament de Ciències Fisiològiques
Universitat de Barcelona
IDIBELL
L'Hospitalet de Llobregat
Barcelona 08907, Spain
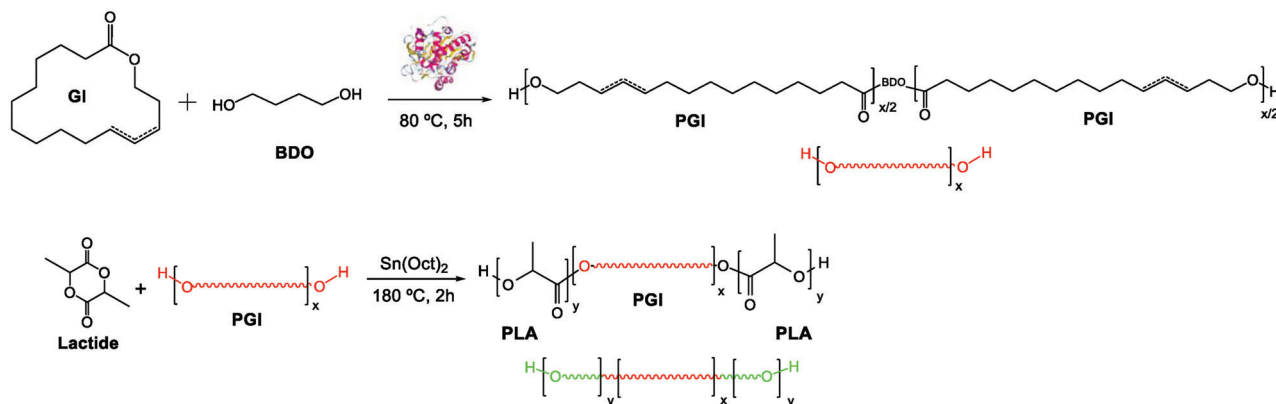
Scheme 1. Synthesis pathway followed to obtain PLA_y-PGl_x-PLA_y triblock copolymers.

Rapidsor (Depuy Synthes), and Bioscrew (ConMed) are some examples. However, they are not temporary grafts as such, but instead they are used for the fixation of autografts, allografts or osteochondral defects. Temporary grafts must be prepared as porous scaffolds to allow bone growth, and nutrients and waste exchange through the pores promoting the healing process.[21–25] But porosity weakens scaffolds,[26] which is critical when using a rigid and brittle polymer such as PLA.

To avoid an undesired fragile fracture, PLA has been reinforced by its combination with softer polyesters. One example of this is PCL, which has a glass transition temperature of −60 °C and displays low strength but extremely high plasticity at tensile stress.[27,28] Blends or block and random copolymers of PLA and PCL proved to avoid the fragile fracture of PLA.[29–31]

But recently, the synthesis of polyesters from lactones with larger ring sizes ($C > 12$) has emerged showing a huge potential.[32] These macrolactones can be obtained from renewable resources[33–36] and are biocompatible as well.[37] Furthermore, the resultant polymers, polymacrolactones (PMLs), are potentially degradable by the hydrolysis of the repeating ester linkage of their backbone, making them suitable for tissue regeneration. The use of PMLs for the plasticization of PLA is very incipient, but they have proved their value. For instance, poly(ω-pentadecalactone) (PPDL) is a PML with a 15-carbon length repeating unit that offers great plasticity and thermal stability. It improved the elongation at break of PLA when both polyesters were blended.[38–40] Besides PPDL, unsaturated PMLs such as poly(globalide), poly(6-ω-hexadecenlactone), or poly(ambrettolide) are remarkable because of the extra functionalization site they present. The double bond could be used to graft bioactive molecules or to prepare antimicrobial polyesters through thiol–ene click reactions, derivatize through epoxidation reactions or even obtain crosslinked networks.[41–45]

The combination of unsaturated PMLs and PLA is still short since, up to our knowledge, only the synthesis of PLA and poly(6-ω-hexadecenlactone) block copolymers has been reported.[46] For that reason, the aim of our study is to recognize these multifunctional copolymers among the conventional biomaterials used for tissue engineering applications. We propose the synthesis of unique PLA-PGl-PLA triblock copolymers with the intent to prepare multifunctional scaffolds. We also describe the end-chain functionalization of the copolymers with PEG and RGD peptides.

PEG was used to increase the hydrophilicity of the copolymers and to act as a nonfouling agent, while the RGD tripeptide was grafted to the surface of the scaffolds to enhance the cell adhesion. The double bonds of PGl blocks were not exploited in this work but is the mission for future research. In fact, our research group has already validated the functionalization of unsaturated polymacrolactones with polypeptides via thiol–ene reactions and it might be valuable for these triblock copolymers.[47–49]

2. Results and Discussion

2.1. Synthesis of Triblock Copolyesters

The synthesis pathway to obtain PLA-PGl-PLA triblock copolymers is depicted in **Scheme 1**. First, a series of hydroxyl ended PGls with a target number average molar mass of 10, 15, 20, and 25 kg mol^{-1} was synthetized. Molar mass was controlled with the monomer-to-initiator ratio. The number average molar mass of synthetized PGls was calculated from nuclear magnetic resonance (NMR) spectroscopy and gel permeation chromatography (GPC). Table S1 (Supporting Information) compiles the results of the molar mass and other relevant data obtained from the synthesis of PGls. The results of NMR spectroscopy were in good agreement with the target values, but GPC seemed to overestimate them. It was speculated that PGl adopted a particular conformation in solution, with a higher hydrodynamic volume than the standards employed, which made them pass through the column faster than they should. Dispersities of PGls was within 1.5–2.0, which are typical values for enzymatic ROPs.[41,50]

Synthetized PGls were then used as macroinitiators in the ROP of lactide. Results of copolymerization reactions are shown in **Table 1**, while **Figure 1** shows a representative ^{1}H NMR spectrum of the copolymers. The broad triplet signals appearing at 3.65 ppm due to the methylene end groups ($-CH_2-OH$) of PGl shifted to 4.15 ppm after the reaction with lactide, appearing partially overlapped with the signal of the oxymethylene ester of PGl (Figure S1, Supporting Information). Shifting was ascribed to the new less shielded environment of the oxymethylene protons as a result of the ester group formation ($-CH_2-O-CO-$). Since no peaks of methylene end groups of PGl were observed after the reaction, it was concluded all PGl chains acted as initiators

2300066 (2 of 14)

Table 1. Composition, conversion, and average molar masses of PLA_γ-PGl_x-PLA_γ copolyesters.

Copolyester	$[LA]^{a)}$ [mol%]	$[Gl]^{a)}$ [mol%]	$X^{a)}$ [%]	$M_n{}^{a)}$ [kg mol^{-1}]	$M_n{}^{b)}$ [kg mol^{-1}]	$M_w{}^{b)}$ [kg mol^{-1}]	$Đ^{b)}$
$PLLA_{184}$-PGl_{43}-$PLLA_{184}$	89.5	10.5	95.7	28.7	29.2	37.5	1.3
$PLLA_{115}$-PGl_{62}-$PLLA_{115}$	78.8	21.2	98.9	29.5	37.2	54.0	1.5
$PLLA_{92}$-PGl_{87}-$PLLA_{92}$	67.9	32.1	94.9	31.4	38.5	60.5	1.6
$PLLA_{42}$-PGl_{102}-$PLLA_{42}$	45.2	54.8	92.8	29.6	34.2	66.5	1.9
$PDLLA_{178}$-PGl_{43}-$PDLLA_{178}$	89.2	10.8	96.6	35.9	45.1	65.6	1.5
$PDLLA_{135}$-PGl_{62}-$PDLLA_{135}$	81.3	18.7	97.1	36.8	44.6	71.0	1.6
$PDLLA_{80}$-PGl_{87}-$PDLLA_{80}$	64.8	35.2	94.1	32.2	37.0	65.4	1.8
$PDLLA_{67}$-PGl_{102}-$PDLLA_{67}$	56.8	43.2	95.0	34.0	39.6	72.3	1.8

a) Molar composition of lactic acid ([LA]) and globalide ([Gl]) in the precipitated copolyesters, lactide conversion (X) and number average molar mass (M_n) calculated from ^{1}H NMR spectra; b) Number average (M_n) and weight average (M_w) molar mass, and dispersity ($Đ$) determined by GPC.
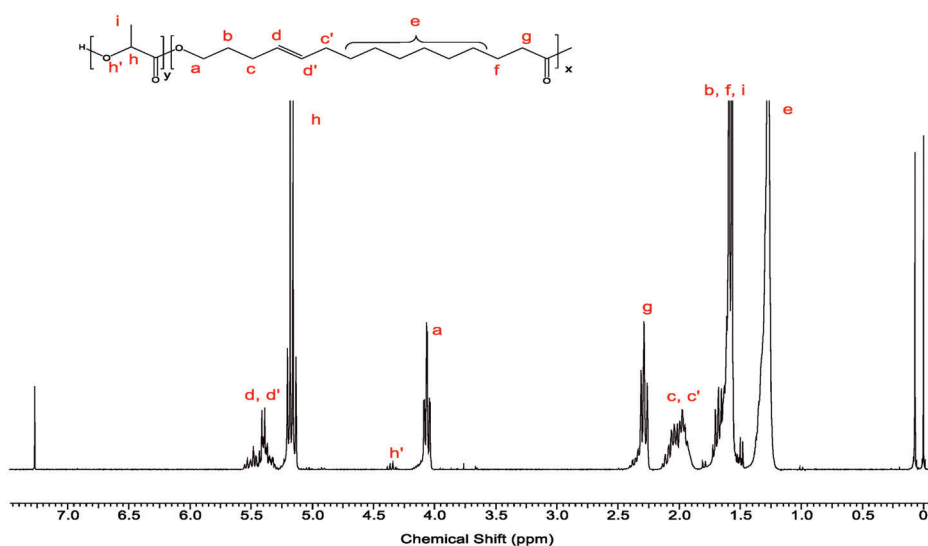
Figure 1. ^{1}H NMR spectrum of $PLLA_{115}$-PGl_{62}-$PLLA_{115}$ with peak assignments. Only one of the positional isomers of PGl is represented.

of lactide polymerization giving as a result the formation of a triblock copolymer.

Same conclusion was obtained from DOSY NMR spectra (Figure S2, Supporting Information). These spectra showed a diffusion coefficient for the copolymer ($D_2 = -10.8$ log(m^2 s^{-1})) that was different from the PGl homopolymer used as macroinitiator ($D_1 = -10.6$ log(m^2 s^{-1})), which confirms that PGl reacted with lactide to form a triblock copolymer. As in other similar systems, slight differences in the diffusion coefficient of each block were observed.[51]
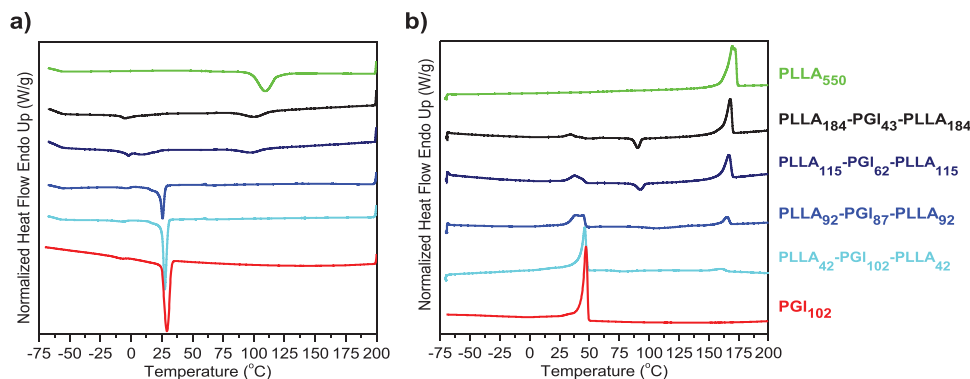
Further evidence of the triblock structure formation was obtained by ^{13}C NMR spectroscopy (Figure S3, Supporting Information) and GPC (Figure S4, Supporting Information). Regarding ^{13}C NMR spectroscopy, it was of particular interest the region between 166 and 177 ppm where signals due carbonyl carbons appear. These carbons are very sensitive to the microstructure and sequence distribution effects. The signals of PLA and PGl homopolymers remained unaltered after copolymerization, which proved that not transesterification took place during the ROP, maintaining the copolyesters the triblock structure. In addition, no spiting of the carbonyls of lactic units

was observed, at least for ʟ-lactide polymerization, indicating that no racemization took place during this process.

Likewise, GPC chromatograms showed evidence of the triblock formation. NMR proved all PGl and all lactide had reacted, but partial homopolymerization of lactide could have occurred due to water or impurity traces producing a mixture of triblock copolymer chains and PLA oligomers. This situation was discarded since the copolymers displayed monomodal distributions, meaning all lactide polymerized from PGl chains. Otherwise, bimodal distributions or shoulders would have been noticed. Furthermore, it was observed a slight increase of the molar mass accompanied by a decrease of the dispersity after copolymerization. It is true that the shift of the monomodal signal towards a higher molar mass is not significant, but it can be explained by the different hydrodynamic volumes of PGl homopolymers and the triblock copolymers.[52]

2.2. Thermal Properties

The thermal properties were evaluated to find out if the triblock structure altered the thermal behavior of the homopolymers

ADVANCED
SCIENCE NEWS
www.advancedsciencenews.com

acro-
molecular
Bioscience
www.mbs-journal.de

Figure 2. DSC traces of PLLA, PGl, and PLLA$_y$-PGl$_x$-PLLA$_y$ copolyesters. a) First cooling and b) second heating at 10 °C min^{-1}.
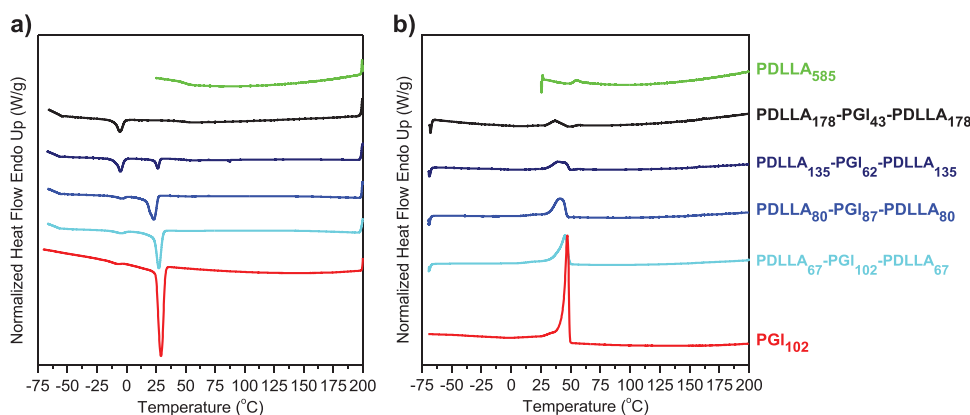
Figure 3. DSC traces of PDLLA, PGl, and PDLLA$_y$-PGl$_x$-PDLLA$_y$ copolymers. a) First cooling and b) second heating at 10 °C min^{-1}.

PGl and PLA. Differential scanning calorimetry (DSC) traces of the synthetized triblock copolyesters and the respective homopolyesters are shown in **Figures 2** and **3**. These thermograms contain the cooling and the heating traces recorded from 200 to −70 °C after the removal of the thermal history of the samples. All data collected from DSC thermograms are displayed in Table S2 (Supporting Information).

PGl displayed a sharp melting peak and also a well-defined crystallization peak at 48 and 32 °C, respectively, which is consistent with previous research.[41,53] Enthalpy changes recorded for both thermal transitions proved that PGl recovered its initial crystallinity during the cooling trace after being melted. Such high crystallinity degree did not allow the detection of the T_g in the thermograms. Quenching of PGl was also evaluated to limit the formation of crystals, though it resulted to be ineffective to detect the glass transition temperature.

On the other hand, PLLA had the melting point at 170 °C. The peak was broader than the one of PGl. In the cooling trace it was appreciable that rearrangement of PLLA chains was more limited. Because of that, it displayed a broad crystallization peak. In the case of PDLLA no first-order transition was observed due to the absence of crystalline regions (Figure 3). The T_g of PLLA and PDLLA was around 57.1 and 53.2 °C, respectively, which agreed expected values as observed from previous studies.[54]

The thermal transitions corresponding to PGl and PLA were observed in the copolyesters, meaning that the repeating units of both polymers were organized in blocks. The block length influenced the thermal transitions, both temperatures and enthalpies, independently of the block nature. The longer block the larger crystalline domains and enthalpy changes. Similarly, the melting or crystallization of the longer blocks required higher temperatures, while the contrary was observed for the shorter blocks. In the literature are found examples of ABA triblock copolymers with PLA displaying similar performances.[55–57] In fact, crystallization of very short blocks was quite problematic and both PLLA and PGl blocks displayed broader crystallization peaks with decreasing block length. PGl even showed separated crystallization peaks in the case of short and medium length block samples, that could be ascribed to the formation of crystals with different lamellar sizes. On the side of PLLA block, it had a more restricted crystallization due to the presence of the PGl mid-block. As it can be observed in Figure 3, the copolyesters displayed cold crystallization peaks at around 100 °C ascribed to the block of PLLA, a behavior that was not observed for the homopolymer.

The thermal decomposition of the triblock copolyesters under inert atmosphere was examined by thermogravimetric analysis (TGA) within the range of 50–600 °C. Relevant data such as the weight loss, the onset temperature at 5% of weight loss ($^oT_d{}^{5\%}$), the maximum rate decomposition temperature ($^{max}T_d$), and the residual weight (R_w) are shown in **Table 2**. Thermograms and their respective derivative curves were included in Figure S5 (Supporting Information).

Table 2. Thermogravimetric analysis of PLAs, PGls, and synthetized triblock copolymers.

Polymer	Weight loss[a]		$^{o}T_d{}^{5\%a)}$	$^{max}T_{d,1}{}^{a)}$	$^{max}T_{d,2}{}^{a)}$	$R_w{}^{a)}$
	1st step [wt%]	2nd step [wt%	[°C]	[°C]	[°C]	[%]
PLLA$_{450}$	98.1	–	263.1	304.4	–	1.9
PDLLA$_{500}$	98.7	–	262.7	303.1	–	1.3
PGl$_{102}$	–	98.2	389.4	–	423.5	1.2
PLLA$_{184}$-PGl$_{43}$-PLLA$_{184}$	68.8	29.7	270.6	319.6	414.6	1.5
PLLA$_{115}$-PGl$_{62}$-PLLA$_{115}$	54.7	45.0	268.5	318.0	415.2	0.3
PLLA$_{92}$-PGl$_{87}$-PLLA$_{92}$	38.6	60.0	275.1	301.4	421.0	1.4
PLLA$_{42}$-PGl$_{102}$-PLLA$_{42}$	19.2	80.5	283.3	297.7	419.6	0.3
PDLLA$_{178}$-PGl$_{43}$-PDLLA$_{178}$	70.7	29.1	261.8	299.9	421.1	0.2
PDLLA$_{135}$-PGl$_{62}$-PDLLA$_{135}$	60.8	38.7	260.7	294.3	422.7	0.5
PDLLA$_{80}$-PGl$_{87}$-PDLLA$_{80}$	32.4	64.1	272.4	293.6	423.6	3.5
PDLLA$_{67}$-PGl$_{102}$-PDLLA$_{67}$	28.8	69.2	278.7	303.2	419.9	2.0

[a] Weight loss, onset for 5% decomposition temperature ($^{o}T_d{}^{5\%}$), maximum rate thermal decomposition temperature of first ($^{max}T_{d,1}$) and second ($^{max}T_{d,2}$) steps, and the remaining weight (R_w) at 600 °C measured by TGA under inert atmosphere.

Table 3. Mechanical properties of PLA$_\gamma$-PGl$_x$-PLA$_\gamma$ copolyesters at tensile stress.

Polymer	[LA][a] [mol%]	$M_w{}^{b)}$ [kg mol^{-1}]	$\sigma_{max}{}^{c)}$ [MPa]	$E^{c)}$ [MPa]	$\gamma_b{}^{c)}$ [%]
PLLA$_{450}$	100	39.8	[d]	[d]	[d]
PDLLA$_{500}$	100	42.1	[d]	[d]	[d]
PGl$_{102}$	–	23.7	4.7 ± 0.2	149 ± 11	420 ± 130
PLLA$_{184}$-PGl$_{43}$-PLLA$_{184}$	89.7	37.5	10.0 ± 3.3	951 ± 66	1.3 ± 0.4
PLLA$_{115}$-PGl$_{62}$-PLLA$_{115}$	79.3	54.0	18.3 ± 1.2	846 ± 62	7.1 ± 1.5
PLLA$_{92}$-PGl$_{87}$-PLLA$_{92}$	68.0	60.5	10.4 ± 1.6	538 ± 46	39.0 ± 25
PLLA$_{42}$-PGl$_{102}$-PLLA$_{42}$	45.4	66.5	4.6 ± 0.5	178 ± 12	250.0 ± 27
PDLLA$_{178}$-PGl$_{43}$-PDLLA$_{178}$	89.2	65.6	22.2 ± 4.7	1090 ± 113	9.2 ± 3.3
PDLLA$_{135}$-PGl$_{62}$-PDLLA$_{135}$	81.3	71.0	21.5 ± 2.1	466 ± 42	200.0 ± 67
PDLLA$_{80}$-PGl$_{87}$-PDLLA$_{80}$	64.5	65.4	11.8 ± 1.2	533 ± 81	260.0 ± 94
PDLLA$_{67}$-PGl$_{102}$-PDLLA$_{67}$	57.0	72.3	9.1 ± 1.1	381 ± 75	330.0 ± 87

[a] Weight composition of PLA calculated from ^{1}H NMR spectra; [b] Weight average molar mass determined by GPC; [c] Maximal tensile strength (σ_{max}), elastic modulus (E) and elongation at break (γ_b) determined by tensile testing; [d] The probes of PLLA$_{450}$ and PDLLA$_{500}$ were broken in the die-cutting process.

PGl displayed a high thermal stability, with a steep weight loss at 423 °C, yielding a minimal residue at 600 °C, which is typical behavior of aliphatic polyesters derived from macrolactones.[47,58] Both PLAs revealed a very similar thermal decomposition profile, which occurred in a single step and reached the maximum rate of decomposition at around 300 °C. Likewise, neither of the PLAs remained with a significant weight at the end of the assays.

The triblock copolymers decomposed in two steps, according to the two repeating units of the block structure. The thermograms were very clear because the decomposition temperatures of the blocks were quite separated. Such difference allowed the calculation of the weight loss of each block, which was in good agreement with the composition determined by ^{1}H NMR.

2.3. Mechanical Properties

The mechanical properties of the triblock copolymers and representative homopolymers were determined by tensile tests fol-lowing the standard UNE-EN ISO 527-1. The results of the maximum tensile strength (σ_{max}), the elastic modulus (E), and the elongation at break (γ_b) are depicted in **Table 3**. Both PLLA and PDLLA films could not be tested due to their excessive brittleness. PLA is known to be a brittle material that barely deforms a 2%–10% before failure with a maximal tensile strength of about 50–70 MPa and an elastic modulus of 3000–4000 MPa.[59] In this case, and probably due to the moderate molar mass ($M_w \approx 40$ kg mol^{-1}), it could not even support the stress generated by the die cutter.

On the other hand, the stress–strain curves of PGl exhibited a great plastic behavior. Figure S6 (Supporting Information) shows a representative curve of PGl tensile performance, in which the three most typical distinctive response zones of plastic materials were identified: i) elastic response, ii) plastic deformation, and iii) strain hardening. The elastic response of PGl resulted in relatively high deformations and a low elastic modulus ($E \approx$ 149 MPa). Elastic deformation mainly occurs by the interlamellar
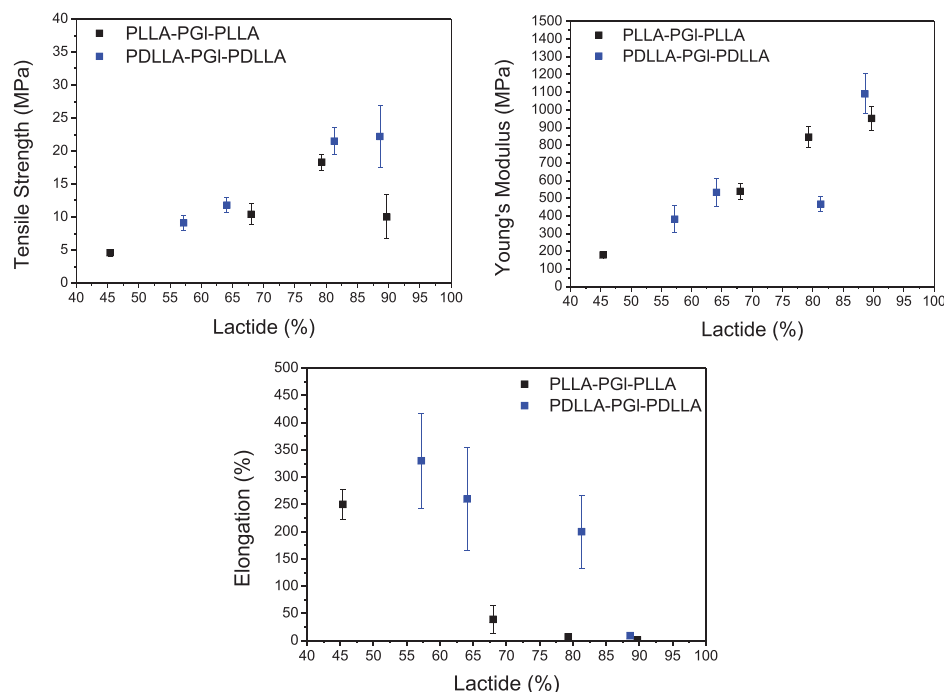
Figure 4. Tensile performance of PLA$_\gamma$-PGl$_x$-PLA$_\gamma$ copolyesters.

shearing of the amorphous phase and they had a great mobility because the tests were performed above the T_g of PGl.[60] But in the yield point ($\sigma_Y \approx 4.7$ MPa, $\gamma_Y \approx 10\%$), the inability to transfer the stress beyond the crystallite's boundaries led to lamellae splitting and fragmentation into blocks, giving way to plastic deformation and necking of specimen tests.[61–63] The highlight of PGl stress-strain curves was precisely that, the plastic deformation occurring from 10% to 300%, when neck propagation and easy plastic flow of the specimen tests were noticed. Throughout this region, the great mobility of the amorphous phase was recovered owing to lamellae fragmentation and crystal slipping after the yield point, which allowed the orientation of the amorphous phase in the direction of the stress with relatively low stress requirement. However, above $\gamma \approx 350\%$, the increasing entanglement density of the amorphous phase made necessary more stress to continue straining the polymer. Neck propagation was yet notorious at this stage and whitening became more evident as the formation of voids in the amorphous phase during crystallite fragmentation and deformation.[64,65] Such phenomenon is known as strain-hardening and it is independent of the crystallinity degree.[60] Finally, cumulative void formation and the inability to transfer the stress led to failure.[66]

The plastic behavior of PGl was thought to be beneficial to strengthen PLA and avoid the brittle fracture. A range of compositions were evaluated to observe how it influenced the mechanical properties of the copolyester. The relationship between σ_{max}, E, and γ_b with the content of lactide is depicted in **Figure 4**. Representative stress–strain curves of the triblock copolymers are shown in Figure S7 (Supporting Information). As observed, all the parameters followed a certain tendency with increasing content of lactide. Longer blocks of PGl supplied to the triblock copolymers the ability to undergo plastic deformation
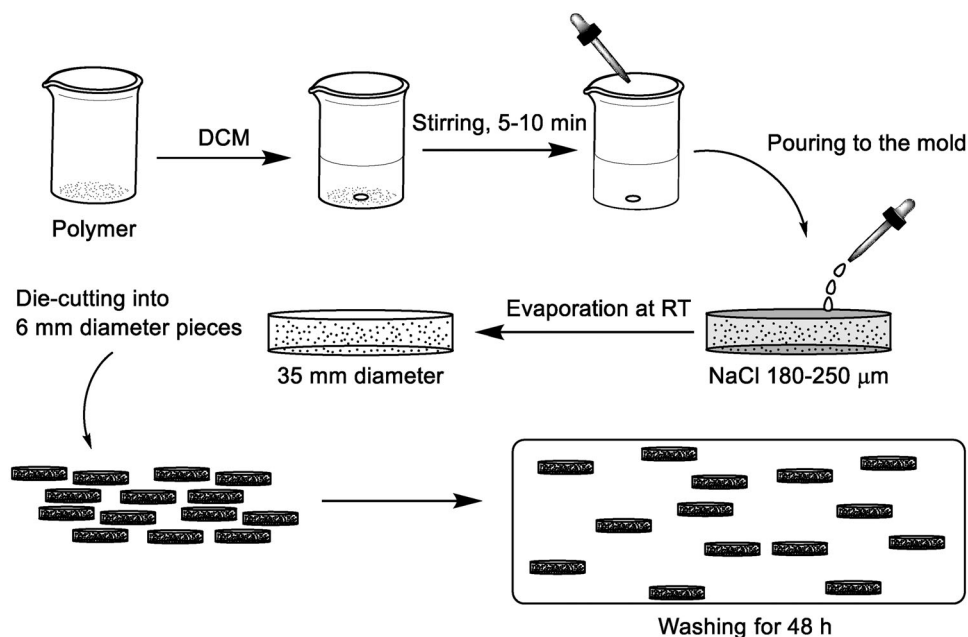
prior to failure. Instead, longer blocks of PLA increased the tensile strength and the elastic modulus almost fitting a linear relationship. It is worth to remember that neat PLAs of moderate M_w did not resist the stress of the die-cutter, thus copolymerization with PGl truly plasticized PLA-based copolymers at any of the evaluated compositions.

Besides the influence of the block length in the tensile performance, it was noticed that stereochemistry of PLA blocks was also relevant. Not in the case of the tensile strength nor the elastic modulus, which were very similar, but in the plastic deformation they experienced prior to failure. The total absence of crystalline domains in PDLLA blocks provided more freedom to the chain arrangement throughout the tensile stress, resulting in larger plastic deformations. Therefore, the overall tensile performance of copolymers containing PDLLA blocks was superior.

The mechanical properties of PEGylated copolymers were also evaluated under tensile stress. Figure S8 (Supporting Information) compares the curves of a PLA$_\gamma$-PGl$_x$-PLA$_\gamma$ copolymer before and after PEGylation. As expected, the incorporation of PEG chains plasticized the triblock copolymer.[67,68] Elongation at break was enhanced and elastic module was reduced because of PEGylation.

2.4. PEG Functionalization of Triblock Copolymers

After the initial evaluation of the series of triblock copolymers, only those containing the shorter blocks of PGl (PGl$_{43}$ and PGl$_{62}$) were selected for further functionalization. The selection was based on the mechanical properties of these polymers. It was proved that shorter PGl blocks were enough to provide PLA with certain ductility. In addition, it was taken into account that PEGy-

**ADVANCED
SCIENCE NEWS**

www.advancedsciencenews.com

**[M] acro-
molecular
Bioscience**

www.mbs-journal.de

Scheme 2. Representation of the scaffold preparation process by the solvent-casting and particulate leaching technique.

lation would further improve the plastic behavior of the copolymers, thus seemed reasonable to select the copolymers with shorter PGl blocks. From this point forward, the selected copolymers were renamed as follows: PLLA$_{184}$-PGl$_{43}$-PLLA$_{184}$ as PF01, PLLA$_{115}$-PGl$_{62}$-PLLA$_{115}$ as PF02, PDLLA$_{178}$-PGl$_{43}$-PDLLA$_{178}$ as PF03, and PDLLA$_{135}$-PGl$_{62}$-PDLLA$_{135}$ as PF04.

First of all, PEG hydroxyl end groups were transformed into carboxyl end-groups. For that PEG was made to react with succinic anhydride catalyzed by DMAP. ^{1}H NMR spectrum of the product obtained after purification proved that the reaction was successful (Figure S9, Supporting Information).

The carboxyl-terminated PEG was then linked to the triblock copolymers by Steglich esterification to produce pentablock copolymers (PEG$_z$-PLA$_y$-PGl$_x$-PLA$_y$-PEG$_z$). PEGylated copolymers from PF01, PF02, PF03, and PF04 were named as PF11, PF12, PF13, and PF14, respectively. A fivefold excess of carboxyl-terminated PEG was used to prevent the reaction of a single PEG chain with two triblock copolyester chains. Esterification was confirmed by ^{1}H NMR as the ending groups of PLA blocks disappeared (Figure S10, Supporting Information). Furthermore, the average number of repeating units of PEG calculated from NMR spectra matched the theoretical one (20–24 repeating units) according to the number average molar mass specified by the provider.

2.5. Scaffold Preparation

The scaffolds were prepared by a solvent-casting and particulate leaching technique. The whole procedure is depicted in **Scheme 2**. One of the most relevant parameters in the design of the scaffolds is the interconnectivity between the pores. Isolated pores and closed channels would be a threat for cell survival.[22] To minimize the number of closed channels the scaffolds were

provided with a great porosity (over 90%). Porosity was created using sieved NaCl particles within the 177–250 µm (mesh 60–80) range, which was reported to be the optimal pore size for bone cell survival.[24] Nevertheless, as observed in SEM images of PF04 (**Figure 5**), because of the great porosity and the overlapping of several pores, the average pore size was larger. They might be around 300 µm, but an accurate measurement was tricky due to their different orientation. Moreover, PEGylation of triblock copolymers did not produce any change in the architecture of the scaffolds.

Potential risks of not using the double bond of PGl was the self-crosslinking of PGl blocks or the coloration of the samples after a period of time. But the risks did not materialize, being the polymer totally soluble and colorless after 6 months since they were synthetized.

Reproducibility of scaffolds was evaluated by the weight control of the scaffolds and by SEM images. The average weight of more than 600 prepared scaffolds was 5.0 ± 0.5 mg, which reflected a great consistency on porosity, size, and thickness. In addition, from Figure 5 it was noticed that the scaffolds exhibited a homogeneous pore distribution. Just small defects were observed in both Figure 5c,f. They might have appeared during the transition of the polymer from solution to solid state after the evaporation of the solvent and promoted by the stress caused by NaCl particles. Nonetheless, these defects should not be problematic for the cell activity. Cells would perceive these small defects as plain walls.

2.6. Contact Angle (CA)

Hydrophobicity of the polymers was determined by the measurement of the CA of a water drop in a series of films and scaffolds. The average results and their respective standard deviations are
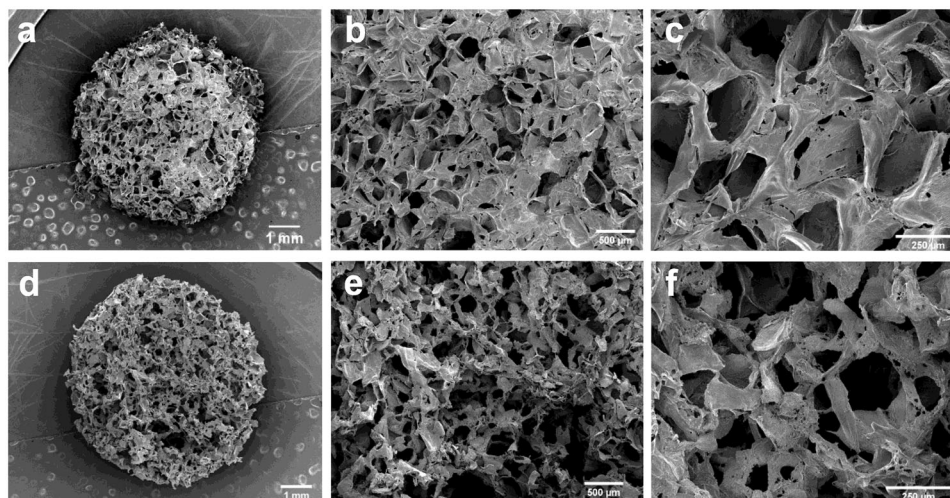
**ADVANCED
SCIENCE NEWS**

www.advancedsciencenews.com

**Macro-
molecular
Bioscience**

www.mbs-journal.de

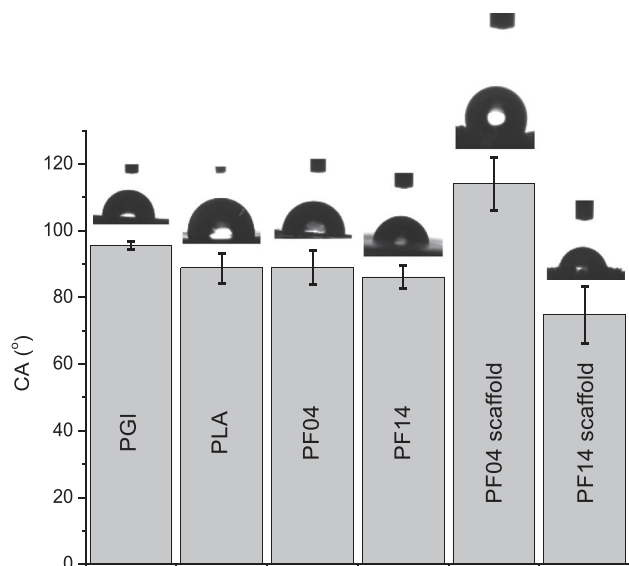**Figure 5.** SEM images of a–c) PF04 and d–f) PF14 at different scales.

Figure 6. Comparison of contact angles of PGl, PLA, PF04, PF14 films, and PF04 and PF14 scaffolds.

depicted in **Figure 6**, which also includes a picture of the water drop in contact with the film or the scaffold. Both PGl and PLA homopolymers were of great interest in order to establish the initial reference and study the influence of the copolymerization (PF04) and the PEG functionalization (PF14).

The CA of PGl and PLA was 95.5° and 88.8°, respectively. Then, the copolymer PF04, containing a 15 mol% of Gl, showed an intermedium value of 89.0°. All of them were close to the 90° limit that is used to elucidate if a material is hydrophobic (CA > 90°) or hydrophilic (CA < 90°). In the case of PGl, hydrophobicity was expected because of its long polymethylene backbone and the absence of polar moieties. PLA and the copolymer PF04, instead, showed a CA just below the limit of 90° and, according to that, they should be considered hydrophilic polymers. However, when PLA is used as implantable medical device, its low

wettability causes the adhesion of nonspecific proteins, promoting the inflammatory response of the body after implantation.[69] It is hence of great interest to provide PLA with hydrophilic moieties as we did by the end-chain functionalization of the copolymers with PEG. Thereby, nonfouling surfaces could be obtained by the formation of a water layer at the surface of the material that is connected by hydrogen bonds.[70]
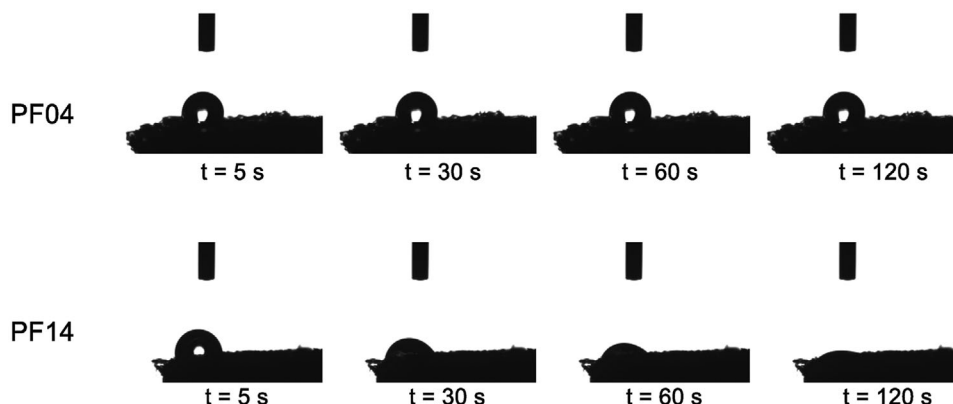
Interestingly, functionalization with PEG ($M_n \approx 1$ kg·mol^{-1}) decreased the CA from 89.0° (PF04) to 86.1° (PF14) in the films. It may seem PEGylation did not produce a significant effect on the wettability of the copolymers, but it is worth noting this slight reduction of 3° in the films was enough to produce hydrophilic scaffolds. While PF04 films displayed a CA of 89.0°, the scaffolds raised the CA to 114°. On the contrary, the CA of PF14 decreased from 86.1° in the films to 74.8° in the scaffolds. This is because the scaffolds have rough surfaces and roughness has a great influence on the wetting behavior. There have been developed different models to explain the relationship between the contact angles and roughness.[71] Briefly, these models demonstrated that flat surfaces accentuated their hydrophobic or hydrophilic character when they were roughened. The CA of PF04 film was very close to the 90° limit, thus the roughening of the surface turned PF04 into a hydrophobic scaffold. In contrast, the reduction of just 3° in the PF14 film was enough to provide hydrophilic scaffolds.

The difference between the wettability of PF04 and PF14 scaffolds was emphasized in the evolution of a water drop at the surface. **Figure 7** shows the comparison of both assays in a time lapse of 120 s. The water drop remained unaltered at the surface of PF04 scaffold. Instead, the water drop penetrated through the porous surface of PF14 scaffold aided by the increased wettability provided by the PEG functionalization.
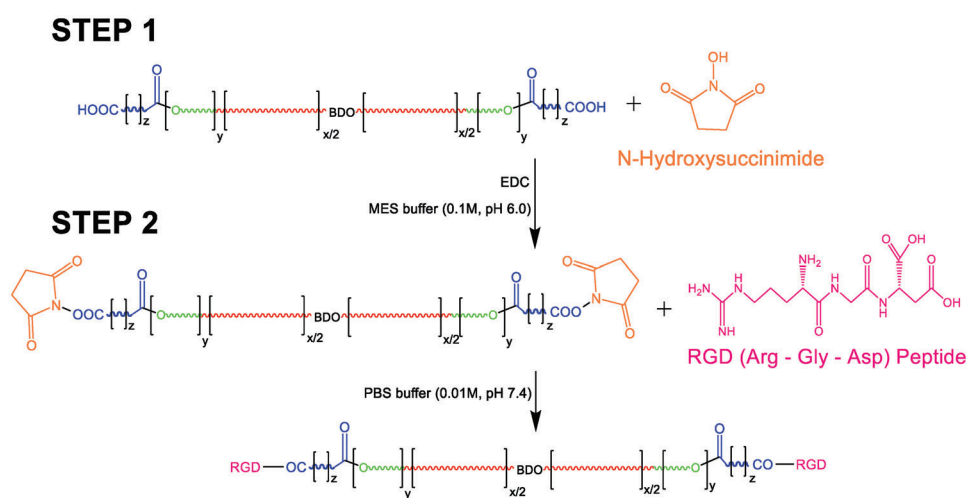
2.7. Functionalization of the Scaffold Surfaces with RGD Peptides

The reaction scheme for the functionalization of scaffold surfaces with RGD peptides is depicted in **Scheme 3**. First, the carboxyl end-groups of PEGylated triblock copolymers located at

ADVANCED
SCIENCE NEWS

www.advancedsciencenews.com

Macro-
molecular
Bioscience

www.mbs-journal.de

Figure 7. Evolution of a water drop at PF04 and PF14 scaffolds surface.

Scheme 3. Reaction scheme of RGD peptide functionalization of PEGylated triblock copolyesters via carbodiimide chemistry. Step 1: activation of carboxyl end-groups of PEGylated triblock copolymers. Step 2: conjugation of the activated carboxyl groups to primary amines of RGD peptides via amide bonds.
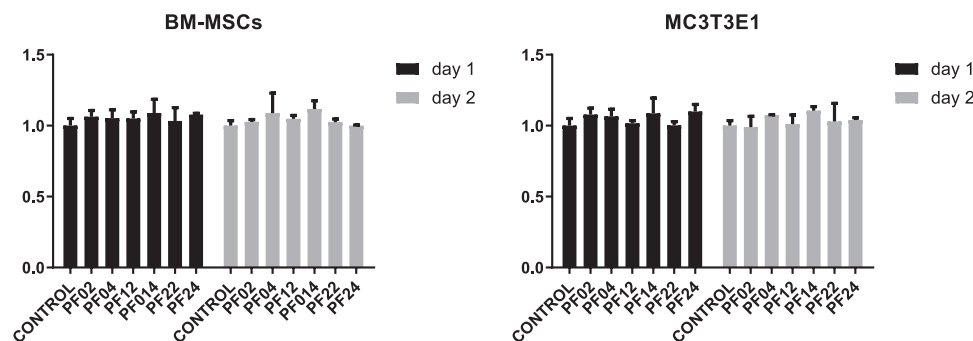
the surface of the scaffolds were activated by carbodiimide chemistry using 1-ethyl-3-(-3-dimethylaminopropyl) carbodiimide hydrochloride (EDC), which is a water soluble carbodiimide (Step 1). Then, the activated carboxyl groups at the surface of the scaffolds reacted with the amino group of the arginine residue of RGD peptides (Step 2). PEGylated triblock copolymers PF11, PF12, PF13, and PF14 were then labeled as PF21, PF22, PF23, and PF24, respectively, after coupling of the RGD peptides.

Yield of the RGD peptide functionalization was determined by ninhydrin tests. These assays were performed to the reaction solutions before and after the coupling of peptides. Ninhydrin changes the color of the solution from light yellow to dark blue when it reacts with amino groups.[72,73] Therefore, those unreacted peptides would react with ninhydrin triggering the change of solutions color. Ultraviolet (UV) spectroscopy was used to determine the number of reacted peptides. **Figure 8** shows the yield of RGD coupling reaction in the synthesis of PF21, PF22, PF23, and PF24. The reproducibility of the reaction was quite consistent. The average yield was about 70%–80%. Only PF23, which partially uncompleted the esterification reaction when
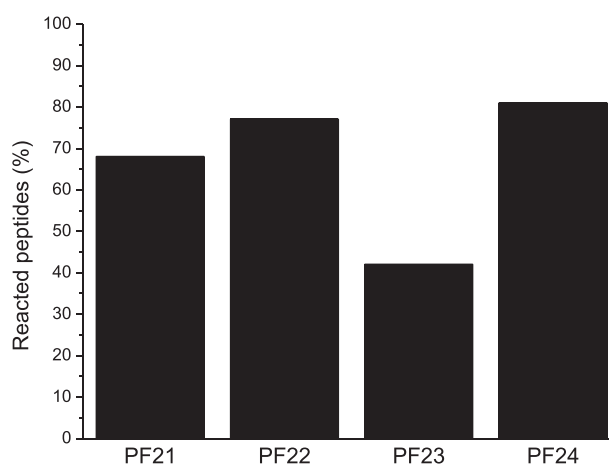

Figure 8. Quantification of reacted RGD peptides.

linking COOH-PEG-COOH to the triblock copolymer (PF13), achieved a lower reaction yield. That was reasonable due to PF13 had less carboxyl functional groups where RGD peptides could be attached.

**ADVANCED
SCIENCE NEWS**

www.advancedsciencenews.com

$\left\{\begin{matrix}M\end{matrix}\right\}$ acro-
olecular
Bioscience

www.mbs-journal.de

Figure 9. Viability of BM-MSCs and MC3T3-E1 cells in the series PFX2 and PFX4 of the scaffolds. Results were expressed as the mean ± standard error of the mean value of three independent experiments.
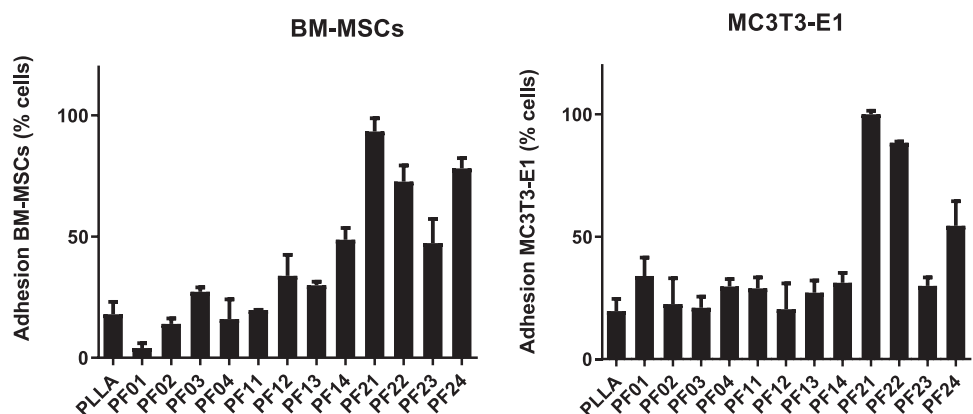
Figure 10. Cell adhesion of BM-MSCs and MC3T3-E1 onto PLLA, PF0X, PF1X, and PF2X scaffolds overnight. Results were expressed as the mean ± standard error of the mean value of five independent experiments.
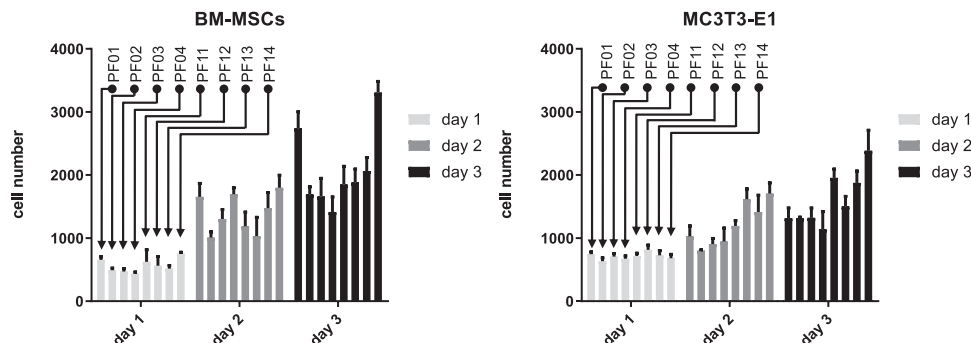
2.8. In Vitro Analysis

The potential of these scaffolds for tissue engineering applications was assessed in vitro by cytotoxicity, cell adhesion and proliferation assays using MC3T3-E1 cell line and bone marrow-derived primary mesenchymal stem cells (BM-MSCs). Cytotoxicity was evaluated using the conditioned media obtained from L-lactide (PF02, PF12, and PF22) and D,L-lactide (PF04, PF14, PF24) scaffolds after 24 h of incubation at 37 °C. **Figure 9** shows the viability of BM-MSCs and MC3T3-E1 cells one and two days after the addition of the conditioned media. The results showed none of the scaffolds compromised the viability of any cell type. The main potential danger was the release of acidic compounds from lactide blocks, but the slow hydrolytic degradation did not threaten cell survival. Complementarily, Figure S11 (Supporting Information) shows the Hoechst staining of BM-MSCs nuclei in nonfunctionalized (PF04) and PEGylated RGD-functionalized scaffolds (PF24). The images showed that cells were viable in the two representative scaffolds.

Then, adhesion of both cell lines onto the scaffolds was evaluated. **Figure 10** shows the ratio of seeded cells that remained adhered after 24 h. Both cell types colonized all the scaffolds. However, copolymer (PF0X) and PEGylated copolymer (PF1X) scaffolds only achieved about a 30% of cell adhesion. This could be explained by the poor cell affinity of PLA, which was already anticipated in previous studies.[74,75] Likewise, those scaffolds

functionalized with PEG were not expected to provide better cell adhesion due to PEG is known to produce anti-fouling surfaces.[70] Conversely, PF2X scaffolds functionalized with cell adhesion RGD peptides outperformed the others reaching a 50%–80% of cell adhesion. This was also observed by triple staining images, in which the colonization and viability of BM-MSCs in both representative PF04 and PF24 were assessed (Figure S12, Supporting Information). The ratio of live/dead cells in both of them was similar, but the cell adhesion in PF24 surpassed PF04. The quantity of living cells adhered to PF24 was higher. This also proved that the surface functionalization of scaffolds with RGD peptides was successfully accomplished, since these peptides are specific to promote cell adhesion.[76–78] Among them, PF23 supplied less adhesion to both cells and it was attributed to the partially uncomplete esterification of PEG achieved when synthetizing PF13 from PF03, which ultimately affected the coupling of RGD peptides to obtain PF23.

Proliferation of BM-MSCs and MC3T3-E1 cells was evaluated at days 1, 2, and 3. These assays were only conducted with PF1X and PF2X scaffolds because the adhesion onto PF0X scaffolds was minimal. Proliferation results are depicted in **Figure 11**. As expected from adhesion experiments, cells were effectively seeded and attached to the surface of the scaffolds. After 1 d, the scaffolds supported the adhesion and proliferation of both cell types, being only slightly lower than the observed on standard coated tissue plates (data not shown). In the following days, PF2X

**ADVANCED
SCIENCE NEWS**

www.advancedsciencenews.com

**[M] acro-
olecular**

Bioscience

www.mbs-journal.de

Figure 11. Proliferation of BM-MSCs and MC3T3-E1 in the PF1X (first 4 bars) and PF2X (last 4 bars) evaluated at day 1, 2, and 3. Results were expressed as the mean ± standard error of the mean value of five independent experiments.

scaffolds nearly achieved the twofold growth associated to the cell division in these specific cell types when cultured in vitro.

These results proved that all the scaffolds had an appropriate architecture in terms of pore size, pore distribution and porosity to promote the proliferation of adhered cells.[22–24,26] Nevertheless, proliferation in of PF24 was notably higher. This was addressed to the softer mechanical properties of PF24 that delivered a more optimal architecture for the proliferation of adhered cells.

3. Conclusions

For the first time PLA-PGl-PLA copolymers have been synthesized, and after derivatization, were used for preparing scaffolds that could have huge potential for tissue engineering applications. The presence of PGl mid-block prevented the brittle fracture of PLA, making the porous scaffolds softer and ductile. The addition of PEG was key for obtaining hydrophilic scaffolds. Functionalization with RGD peptides at the surface was carried out after the preparation of the scaffolds, thus it can be used whatever the technique employed for scaffolding. Moreover, according to the results of the in vitro analysis, these scaffolds are quite promising for the biomedical field. None of them was toxic for BM-MSCs neither for MC3T3-E1 cells, while those scaffolds containing RGD peptides on the surface outperformed the others.

Nevertheless, there is still much research to be done regarding these novel functional polymers. Degradation studies would be necessary to categorize these scaffolds either for short- or long-term treatments. Likewise, the presence of the double bonds in the inner block PGl provide a second place for further functionalization that will be investigated in the future.

4. Experimental Section

Materials: All reagents, unless otherwise specified, were purchased from Sigma-Aldrich and used as received. Globalide was kindly provided by Symrise (Holzminden, Germany). L-lactide (L-LA) (PURASORB L) and D,L-lactide (DL-LA) (PURASORB DL) were gifted by Corbion and dried prior to use in a desiccator under vacuum at 40 °C for 24 h. Novozym 435 biocatalyst (N435, 1.1% w/w of *Candida antarctica* Lipase B immobilized on cross-linked polyacrylate beads) was donated by Novozymes (Bagsværd, Denmark). N435 biocatalyst was stored in a refrigerator and dried in a desiccator at 40 °C under vacuum for 24 h before use. Chloroform, methanol, diethyl ether, and dichloromethane (DCM) were purchased from Labkem

(Barcelona, Spain). Chloroform (99.9%) and tetrahydrofuran (99.9%) GPC solvents were purchased from Across Organics (Geel, Belgium). Deuterated solvent CDCl$_3$ was obtained from Eurolsotop (Saint Aubin, France).

Synthesis of Poly(L-lactide): Poly(lactic acid) was obtained from the ROP of lactide (4 g) at 180 °C. ROP was carried out in a three-necked reactor in bulk, with mechanical stirring and using vacuum and N$_2$ flux to provide an inert reaction atmosphere. The catalyst Sn(Oct)$_2$ was added in a concentration of 0.05 wt% respect to the monomer, while the concentration of the initiator 1,4-butanediol was adjusted to 0.36 mol% to match the target number average molar mass of 40 kg mol^{-1}. The reaction was left to proceed for 2 h. Final reaction mixture was dissolved in chloroform and precipitated in methanol. The precipitate was recovered by filtration, washed with methanol, and dried at 40 °C overnight. Yield = 90%. ^{1}H NMR (300.1 MHz, CDCl$_3$, 25 °C) δ (ppm): 5.17 (m, −CH−), 4.35 (q, −**CH**−OH), 1.58 (d, −CH$_3$). ^{13}C NMR (75.5 MHz, CDCl$_3$, 25 °C) δ (ppm): 169.6 (−C(O)O−), 69.0 (−**C**H−C(O)O−), 16.6 (−CH$_3$).

Synthesis of Polyglobalide: Polyglobalide (PGl) was obtained from the enzymatic ROP in bulk of globalide (4 g) at 80 °C for a reaction time of 5 h. The biocatalyst N435 was used in a concentration of 5 wt% in every experiment, while the initiator, 1,4-butanediol, was varied to control the average molar mass of PGl. Target number average molar mass of PGl was 10, 15, 20, and 25 kg mol^{-1}, which required 2.36, 1.58, 1.18, and 0.95 mol% of initiator, respectively. After polymerization, the mixture was dissolved in chloroform, filtrated to remove the biocatalyst, and precipitated in methanol. Samples were dried under vacuum for 24 h at room temperature before characterization. Yield = 90%. ^{1}H NMR (300.1 MHz, CDCl$_3$, 25 °C) δ (ppm): 5.40 (m, −CH=CH−), 4.06 (t, −CH$_2$O−), 3.64 (m, −**CH$_2$**−OH), 2.29 (t, −CH$_2$−CO−), 2.16–1.92 (m, −**CH$_2$**−CH=), 1.75–1.55 (m, −**CH$_2$**−CH$_2$C(O)− and −**CH$_2$**−CH$_2$O−), 1.20–1.40 (s, −CH$_2$−). ^{13}C NMR (75.5 MHz, CDCl$_3$, 25 °C) δ (ppm): 173.9 (−C(O)O−), 133.5 (−CH=), 131.5 (−CH=), 128.6 (−CH=), 125.0 (−CH=), 63.7 (−C(O)O−**C**H$_2$), 34.3 (−**C**H$_2$−C(O)O), 32.5, 29.54, 29.51, 29.45, 29.42, 29.26, 29.13, 28.84, 28.48, and 29.97 (−CH$_2$−).

Synthesis of Triblock Copolymers: The PLA$_y$-PGl$_x$-PLA$_y$ triblock copolymers were prepared by ROP of either L- or L,D-lactide initiated by the hydroxyl end groups of PGl macroinitiator. Molar composition of PGl and PLA repeating units in the triblock copolyester was adjusted to achieve in every case a target number average molar mass of 40 kg mol^{-1}. The reaction was carried out in bulk for 2 h, under an inert atmosphere, at a temperature of 180 °C. The concentration of Sn(Oct)$_2$ catalyst was kept constant in every reaction at 0.05 wt%. The reaction was finished by cooling the reactor to room temperature and dissolving the mixture in chloroform. Polymers were recovered by precipitation in methanol, dried and stored in a desiccator until further use. Yield = 90%. ^{1}H NMR (300.1 MHz, CDCl$_3$, 25 °C) δ (ppm): 5.40 (m, −CH=CH− (Gl)), 5.17 (m, −CH− (LA)), 4.35 (q, −**CH**−OH (LA)), 4.15 (m, −CH$_2$−OC(O)− (Gl-LA)), 4.06 (t, −CH$_2$O− (Gl)), 2.29 (t, −CH$_2$−CO− (Gl)), 2.16–1.92 (m, −CH$_2$−CH= (Gl)), 1.75–1.55 (m, −**CH$_2$**−CH$_2$C(O)− and −**CH$_2$**−CH$_2$O− (Gl)), 1.58 (d, −CH$_3$ (LA)), 1.20–1.40 (s, −CH$_2$− (Gl)). ^{13}C NMR (75.5 MHz, CDCl$_3$, 25 °C) δ (ppm):

173.9 (−**C**(O)O− (Gl)), 169.6 (−**C**(O)O− (LA)), 133.5 (−CH= (Gl)), 131.5 (−CH= (Gl)), 128.6 (−CH= (Gl)), 125.0 (−CH= (Gl)), 69.0 (−**C**H−C(O)O− (LA)), 63.7 (−C(O)O−**C**H$_2$ (Gl)), 34.3 (−**C**H$_2$−C(O)O (Gl)), 32.5, 29.54, 29.51, 29.45, 29.42, 29.26, 29.13, 28.84, 28.48, and 29.97 (−CH$_2$− (Gl)), 16.6 (−CH$_3$ (LA)).

Synthesis of COOH-PEG-COOH: For the PEG functionalization of tri-block copolyesters, a carboxyl-terminated PEG was prepared from OH-PEG-OH ($M_n \approx 1000$ g mol^{-1}). Briefly, PEG (8.00 g, 8 mmol) and succinic anhydride (1.61 g, 16 mmol) were placed in a round flask provided with a magnetic stirrer and dissolved in DCM (40 mL). DMAP (0.0988 g, 0.8 mmol) was then added to the solution and the reaction was left to proceed at room temperature for 24 h with magnetic stirring. The reaction mixture was poured into an excess of cold diethyl ether (−18 °C). The precipitated was filtrated, washed repeatedly with fresh solvent, and dried under vacuum for 48 h. Yield = 95%. ^{1}H NMR (300.1 MHz, CDCl$_3$, 25 °C) δ (ppm): 4.26 (t, −O−CH$_2$−**CH**$_2$−OC(O)−), 3.64 (s, −O−CH$_2$−CH$_2$−O−), 2.65 (s, −OC(O)−CH$_2$−CH$_2$−C(O)OH).

PEG Functionalization: Four selected triblock copolyesters were functionalized with PEG by esterification with COOH-PEG-COOH. The mixture containing the triblock copolymer (3.00 g, 0.075 mmol) and a five-fold excess of the carboxyl-terminated PEG (0.75 g, 0.75 mmol) were added to a round flask provided with a magnetic stirrer. The mixture was dissolved with 20 mL of DCM for 30 min. Then, dicyclohexyl carbodiimide (DCC) (0.774 g, 3.75 mmol) and 4-(dimethylamino)pyridine (DMAP) (0.018 g, 0.15 mmol) were added to the solution and the reaction was left to proceed for 24 h at room temperature. The reaction mixture was poured into an excess of methanol to remove the unreacted COOH-PEG-COOH and the catalyst. The precipitate was filtrated, washed repeatedly with fresh methanol, then washed repeatedly with cold diethyl ether (−18 °C), and dried under vacuum for 48 h before characterization. Yield = 90%. ^{1}H NMR (300.1 MHz, CDCl$_3$, 25 °C) δ (ppm): 5.40 (m, −CH=CH− (Gl)), 5.17 (m, −CH− (LA)), 4.26 (t, −O−CH$_2$−**CH**$_2$−OC(O)− (EG)), 4.15 (m, −CH$_2$−OC(O)− (Gl-LA)), 4.06 (t, −CH$_2$O− (Gl)), 3.64 (s, −O−CH$_2$−CH$_2$−O− (EG)), 2.65 (m, −OC(O)−CH$_2$−CH$_2$−C(O)OH and −OC(O)−CH$_2$−CH$_2$−C(O)− (EG)), 2.29 (t, −CH$_2$−CO− (Gl)), 2.16–1.92 (m, −**CH**$_2$−CH$_2$C(O)− and −**CH**$_2$−CH$_2$O− (Gl)), 1.75–1.55 (m, −CH$_2$−CH$_3$ (LA)), 1.20–1.40 (s, −CH$_2$− (Gl)).

Scaffold Preparation: Scaffolds were prepared by the solvent-casting/particulate-leaching technique using DCM as solvent and NaCl as porogen. They were prepared with controlled dimensions (diameter: 35 mm, thickness: 1–2 mm), porosity (95%), and pore size (117–250 μm). NaCl particles were sieved and only particles between mesh 60 (250 μm) and 80 (117 μm) were used. Polymer (0.1 g) was dissolved in 1 mL of DCM. Then, solution was pipetted into the mold, where NaCl particles (1.9 g) were previously placed. The mixture was stirred for a few seconds until homogeneous distribution of the particles was achieved. Solvent evaporation was made at room temperature. Afterward, scaffolds were demoulded. Before the particulate-leaching, scaffolds were cut with a die into smaller scaffolds with 6 mm of diameter. These smaller scaffolds were washed for 48 h with distilled water and low stirring. Water was changed twice a day. Finally, the scaffolds were dried in a desiccator at room temperature using a vacuum pump for 8 h.

RGD Functionalization: RGD peptides were coupled to the surface of the scaffolds in a two-step reaction. First, activation of carboxyl groups was performed by carbodiimide coupling reaction. Briefly, 1-Ethyl-3-(3-dimethylaminopropyl)carbodiimide (EDC) (2.40 mg, 0.01250 mmol) and N-hydroxysuccinimide (NHS) (3.60 mg, 0.03125 mmol) were dissolved in 5 mL of 2-(N-morpholino)ethanesulfonic acid (MES) buffer 0.1 M at pH 6.0 at room temperature. Meanwhile, 10 scaffolds (50 mg, 0.00125 mmol) were incubated for 10 min in 20 mL of the MES buffer. Then, scaffolds were transferred to the activating buffer and the coupling reaction was left to proceed for 30 min with low magnetic stirring. After the reaction, scaffolds were washed with fresh MES buffer and surfaces were absorbed before peptides bioconjugation. The second reaction was performed in 6.5 mL of PBS 0.01 M at pH 7.4 containing 0.1 mg mL^{-1} of RGD peptides (0.65 mg, 0.001875 mmol). The amount of RGD added was calculated as the 75% of the stoichiometric value since the reaction was only expected to take place on the scaffold surface. Bioconjugation was carried out for 16 h with

continuous low magnetic stirring. Afterward, scaffolds were washed with fresh PBS to remove unreacted peptides, absorbed, dried under vacuum for 8 h and stored in a desiccator until further use.

Nuclear Magnetic Resonance: Proton (^{1}H) and carbon (^{13}C) spectra were obtained using a Bruker AMX-300 at 25 °C using 300.1 and 75.5 MHz frequencies, respectively, while DOSY spectra were recorded on a 400 MHz Bruker Avance III. Samples were dissolved in CDCl$_3$ and spectra were calibrated against the signal of tetramethylsilane, used as internal reference. 10 and 50 mg of sample were dissolved in 1 mL of the deuterated solvent for the ^{1}H and ^{13}C NMR spectra, recorded with 64 and 1000–10 000 scans, respectively. The DOSY spectra were recorded with eight scans and the samples were prepared with a concentration of 50 mg mL^{-1}.

Gel Permeation Chromatography: It was used to determine the average molar masses using a Waters instrument equipped with RI and UV detectors. HR5E and HR2 Waters linear Styragel columns (7.8 mm × 300 mm, pore size 10^3–10^4 Å) packed with crosslinked polystyrene and protected with a precolumn were used. Samples were prepared by dissolving 1 mg of polymer in 1 mL of either chloroform or tetrahydrofuran solvents. Measurements were performed at 35 °C with a flow rate of 0.5 mL min^{-1}. Average molar masses were calculated against monodisperse polystyrene or poly(methyl methacrylate) standards for samples run in chloroform or tetrahydrofuran, respectively.

Differential Scanning Calorimetry: Thermal transitions of the polymers were evaluated by DSC in a Perkin Elmer DSC 8500 instrument. Thermograms were obtained from ≈5 g of samples under continuous 20 mL min^{-1} nitrogen flux. Standards used for temperature and enthalpy calibration were indium and zinc. The thermal history of the samples was removed in a first heating over their melting temperatures at 10 °C min^{-1}. Crystallization temperatures (T_c) and enthalpies (ΔH_c) were determined in the first cooling at 10 °C min^{-1}. Melting temperatures (T_m) and enthalpies (ΔH_m) were determined in the second heating at 10 °C min^{-1}. Glass transition temperatures (T_g) were determined in a third heating at 20 °C min^{-1} after quenching the sample by cooling at 100 °C min^{-1}. Data of poly(lactic acid) samples were recorded within 25–200 °C, while those samples containing poly(macrolactones) were analyzed from −80 to 200 °C.

Thermogravimetric Analysis: Thermal stability of the polymers was studied within the temperature range of 50–600 °C. Analyses were performed on a Mettler-Toledo TGA/DSC 1 Star System, using 20 mL min^{-1} of nitrogen flux and with a heating rate of 10 °C min^{-1}.

Scanning Electron Microscopy/Energy-Dispersive X-Ray Spectroscopy (SEM/EDS): SEM images were taken with a JEOL JSM-7001F microscopy at 2 kV and 12×, 30×, 100×, 300×, 1000×, and 3000× magnifications. SEM/EDS images and spectra were recorded in an EDS OXFORD X-Max instrument at 20 kV and a magnification of 1000×.

Contact Angles: Drop shape analysis with sessile drops was performed with an optical contact angle equipment OCA 20 (DataPhysics Instruments GmbH, Filderstadt) and SCA20 software. CAs were measured 5 s after 0.500 μL of distilled water were dropped in 3 × 1 cm^2 film samples at room temperature. Values of the left and right CAs were measured and averaged. At least ten measurements were performed in three different film polymer samples. Dynamic CAs were also carried out by taking pictures of the water drop at scheduled times.

Tensile Tests: Mechanical testing was carried out in a 500N zwicki equipment from Zwick Roell. Tensile and elongation data were recorded by the testXpert III software. Tests were performed using 5B standard specimens obtained from polymer films following the standard UNE-EN ISO 527-1. The films with dimensions 4.0 × 4.5 cm were prepared by hot-pressing using an Atlas Series Heated Platens. After hot-pressing, the films were quenched in an ice bath.

Ninhydrin Tests: 5 mg of ninhydrin were dissolved in 10 mL of ethanol. Then, 0.5 mL of that solution and 0.5 mL of the peptide solution were added to a testing tube. Peptide solutions were prepared at 0.10, 0.05, and 0.025 mg mL^{-1}. A blank solution without peptides was prepared as well. The tube was closed and heated at 105 °C for 20 min. Then, the tube was let to reach room temperature for securing complete color development.

Ultraviolet–Visible Spectrophotometry (UV–vis): UV–vis was used to quantify the number of peptides that reacted with carboxyl-functionalized scaffolds. Peptide solutions, after ninhydrin test, were measured using a

10 mm quartz cuvette at 570 nm in a Cecil Aurius Series CE 2021 spectrophotometer.

Murine Bone Marrow Mesenchymal Stem Cells Isolation: Murine BM-MSCs were isolated from six- to eight-week-old C57BL6/J mice. Femurs were dissected and stored in DMEM (Biological Industries) with 100 U mL^{-1} penicillin/streptomycin. Under sterile conditions, soft tissues were cleaned and femur ends were cut. Bone marrow was flushed with media using a 27-gauge needle, and the cell suspension was filtered through a 70-µm cell strainer (BD Falcon) and seeded. Nonadherent cells were discarded after 3 h. Media was replaced every 12 h for up to 72 h. Then, after reaching 70% confluence, cells were washed with warm PBS and lifted by incubation with 0.25% trypsin/0.02% EDTA for 5 min at room temperature. Lifted cells were cultured and expanded.

Cell Culture: The MC3T3-E1 cell line (American Type Culture Collection, Rockville, MD) and primary cultures of BM-MSCs were maintained in Dulbecco's Modified Eagle's Medium (DMEM) supplemented with 10% fetal bovine serum (FBS), 0.2×10^{-3} M glutamine, 0.1×10^{-3} M pyruvate, and 100 U mL^{-1} penicillin/streptomycin.

Cytotoxicity Analysis: Cytotoxicity measurements were performed to analyze whether different types of scaffolds were cytotoxic as they might release toxic compounds to their environment. MC3T3-E1 and primary cultures of BM-MSCs were seeded in 48-well dishes at a density of 5000 cells per well. After 6 h to obtain cell adhesion to the dish, media was changed to conditioned media from scaffolds incubated with media for 24 h or control media. Viability of cells was measured after 24 and 48 h of treatment with the conditioned media with Alamar blue reagent (Thermofisher Scientific) according to the manufacturer´s instructions. This procedure detects metabolically living cells and automatically quantifies their number. The ratio of living cells in the distinct conditioned media versus control media is displayed in the corresponding graph. For the cytotoxicity imaging analysis, a Hoechst 33342 (Invitrogen) staining was performed following the manufacturer's instructions after 6 h of cell seeding.

Cell Adhesion Tests: Adherence to the distinct scaffolds was determined as follows: scaffolds were introduced into the wells of untreated, low-attachment, 48-well dishes. MC3T3-E1 and BM-MSCs were seeded into the scaffolds at a density of 10 000 cells (in 150 µL of media) per scaffold. After 6 h, scaffolds were gently moved to new dishes and bound cells were quantified with Alamar blue reagent (Thermofisher Scientific) according to the manufacturer's instructions. This procedure detects metabolically living cells and automatically quantifies their number. Percentage of bound cells into the scaffolds is displayed in the corresponding graph. Complementally, viability of adhered cells was analyzed after 6 h of cell seeding. Triple staining with Calcein AM (Millipore) to identify living cells and with iodure propidium (IP) to identify dead cells was performed. Seeded scaffolds were analyzed under confocal laser scanning microscope (Zeiss LSM880).

Cell Proliferation: To assess proliferation of cells on the scaffolds, MC3T3-E1 and BM-MSCs were seeded into the scaffolds at a density of 500 cells (in 150 µL of media) per scaffold as described above. After 6 h, scaffolds were moved to new wells and cultured in 500 µL of media for different times. After 24, 48, or 72 h, cell number was determined with Alamar blue reagent (Thermofisher Scientific) according to the manufacturer´s instructions. Number of cells grown in the different scaffolds is displayed in the corresponding graph.

Statistical Analysis: Quantitative data are presented as mean values ± standard error of the mean value.

Supporting Information

Supporting Information is available from the Wiley Online Library or from the author.

Conflict of Interest

The authors declare no conflict of interest.

Data Availability Statement

The data that support the findings of this study are available in the supplementary material of this article.

[1] A. D. Bagde, A. M. Kuthe, S. Quazi, V. Gupta, S. Jaiswal, S. Jyothilal, N. Lande, S. Nagdeve, *IRBM* **2019**, *40*, 133.

[2] S. W. S. Laurie, L. B. Kaban, J. B. Mulliken, J. E. Murray, *Plast. Reconstr. Surg.* **1984**, *73*, 933.

[3] J. C. Banwart, M. A. Asher, R. S. Hassanein, *Spine* **1995**, *20*, 1055.

[4] H. Shegarfi, O. Reikeras, *J. Orthop. Surg.* **2009**, *17*, 206.

[5] N. Shibuya, D. C. Jupiter, *Clin. Podiatr. Med. Surg.* **2015**, *32*, 21.

[6] W. Wang, K. W. K. Yeung, *Bioact. Mater.* **2017**, *2*, 224.

[7] C. Vacanti, *J. Cell. Mol. Med.* **2006**, *1*, 569.

[8] D. Pappalardo, T. Mathisen, A. Finne-Wistrand, *Biomacromolecules* **2019**, *20*, 1465.

[9] L. L. Hench, J. M. Polak, *Science* **2002**, *295*, 1014.

[10] B. D. Ratner, *J. Cardiovasc. Transl. Res.* **2011**, *4*, 523.

[11] C. Dong, Y. Lv, *Polymers* **2016**, *8*, 42.

[12] F. Croisier, C. Jérôme, *Eur. Polym. J.* **2013**, *49*, 780.

[13] Z. Sheikh, S. Najeeb, Z. Khurshid, V. Verma, H. Rashid, M. Glogauer, *Materials* **2015**, *8*, 5744.

[14] E. Castro-Aguirre, F. Iñiguez-Franco, H. Samsudin, X. Fang, R. Auras, *Adv. Drug Delivery Rev.* **2016**, *107*, 333.

[15] K. A. M. Thakur, R. T. Kean, E. S. Hall, J. J. Kolstad, E. J. Munson, *Macromolecules* **1998**, *31*, 1487.

[16] K. A. M. Thakur, R. T. Kean, E. S. Hall, J. J. Kolstad, T. A. Lindgren, M. A. Doscotch, J. I. Siepmann, E. J. Munson, *Macromolecules* **2002**, *30*, 2422.

[17] J. E. Kasperczyk, *Macromolecules* **1995**, *28*, 3937.

[18] H. Tsuji, Y. Ikada, *J. Appl. Polym. Sci.* **1997**, *63*, 855.

[19] X. Zhang, M. Espiritu, A. Bilyk, L. Kurniawan, *Polym. Degrad. Stab.* **2008**, *93*, 1964.

[20] S. Farah, D. G. Anderson, R. Langer, *Adv. Drug Delivery Rev.* **2016**, *107*, 367.

[21] P. Chocholata, V. Kulda, V. Babuska, *Materials* **2019**, *12*, 568.

[22] G. Turnbull, J. Clarke, F. Picard, P. Riches, L. Jia, F. Han, B. Li, W. Shu, *Bioact. Mater.* **2018**, *3*, 278.

[23] N. Abbasi, S. Hamlet, R. M. Love, N.-T. Nguyen, *J. Sci.: Adv. Mater. Devices* **2020**, *5*, 1.

ADVANCED
SCIENCE NEWS
www.advancedsciencenews.com

Macromolecular
Bioscience
www.mbs-journal.de

[24] X. Chen, H. Fan, X. Deng, L. Wu, T. Yi, L. Gu, C. Zhou, Y. Fan, X. Zhang, *Nanomaterials* **2018**, *8*, 960.

[25] S. Stratton, N. B. Shelke, K. Hoshino, S. Rudraiah, S. G. Kumbar, *Bioact. Mater.* **2016**, *1*, 93.

[26] C. M. Murphy, M. G. Haugh, F. J. O'brien, *Biomaterials* **2010**, *31*, 461.

[27] D. B. Konwar, J. Jacob, B. K. Satapathy, *Polym. Int.* **2016**, *65*, 1107.

[28] B. Torabinejad, J. Mohammadi-Rovshandeh, S. M. Davachi, A. Zamanian, *Mater. Sci. Eng., C* **2014**, *42*, 199.

[29] C. Zhang, T. Zhai, L.-S. Turng, Y. Dan, *Ind. Eng. Chem. Res.* **2015**, *54*, 9505.

[30] J. Fernández, A. Etxeberria, J.-R. Sarasua, *J. Mech. Behav. Biomed. Mater.* **2012**, *9*, 100.

[31] M. Naddeo, A. Sorrentino, D. Pappalardo, *Polymers* **2021**, *13*, 627.

[32] J. A. Wilson, Z. Ates, R. L. Pflughaupt, A. P. Dove, A. Heise, *Prog. Polym. Sci.* **2019**, *91*, 29.

[33] T. Fortunati, M. D'acunto, T. Caruso, A. Spinella, *Tetrahedron* **2015**, *71*, 2357.

[34] A. S. Williams, *Synthesis* **1999**, *1999*, 1707.

[35] A. Sytniczuk, A. Leszczyńska, A. Kajetanowicz, K. Grela, *ChemSusChem* **2018**, *11*, 3157.

[36] J. A. Wilson, S. A. Hopkins, P. M. Wright, A. P. Dove, *Biomacromolecules* **2015**, *16*, 3191.

[37] H. T. H. Nguyen, G. N. Short, P. Qi, S. A. Miller, *Green Chem.* **2017**, *19*, 1877.

[38] M. P. F. Pepels, W. P. Hofman, R. Kleijnen, A. B. Spoelstra, C. E. Koning, H. Goossens, R. Duchateau, *Macromolecules* **2015**, *48*, 6909.

[39] A. M. Ziemba, K. P. Lane, I. M. San Segundo, A. R. D'amato, A. K. Mason, R. J. Sexton, H. Casajus, R. A. Gross, D. T. Corr, R. J. Gilbert, *ACS Biomater. Sci. Eng.* **2018**, *4*, 1491.

[40] R. Todd, S. Tempelaar, G. Lo Re, S. Spinella, S. A. Mccallum, R. A. Gross, J.-M. Raquez, P. Dubois, *ACS Macro Lett.* **2015**, *4*, 408.

[41] Z. Ates, P. D. Thornton, A. Heise, *Polym. Chem.* **2011**, *2*, 309.

[42] Z. Ates, A. Heise, *Polym. Chem.* **2014**, *5*, 2936.

[43] C. L. Savin, C. Peptu, Z. Kroneková, M. Sedlačík, M. Mrlik, V. Sasinková, C. A. Peptu, M. Popa, J. Mosnáček, *Biomacromolecules* **2018**, *19*, 3331.

[44] M. Naddeo, G. Vigliotta, C. Pellecchia, D. Pappalardo, *React. Funct. Polym.* **2020**, *155*, 104714.

[45] F. C. S. De Oliveira, D. Olvera, M. J. Sawkins, S-A. Cryan, S. D. Kimmins, T. E. Da Silva, D. J. Kelly, G. P. Duffy, C. Kearney, A. Heise, *Biomacromolecules* **2017**, *18*, 4292.

[46] T. Fuoco, A. Meduri, M. Lamberti, V. Venditto, C. Pellecchia, D. Pappalardo, *Polym. Chem.* **2015**, *6*, 1727.

[47] E. Tinajero-Díaz, A. Martínez de Ilarduya, B. Cavanagh, A. Heise, S. Muñoz-Guerra, *React. Funct. Polym.* **2019**, *143*, 104316.

[48] E. Tinajero-Díaz, A. Martínez de Ilarduya, S. Muñoz-Guerra, *Polymers* **2020**, *12*, 995.

[49] E. Tinajero-Díaz, A. Martínez de Ilarduya, S. Muñoz-Guerra, *Macromol. Chem. Phys.* **2019**, *220*, 17.

[50] M. P. F. Pepels, P. Souljé, R. Peters, R. Duchateau, *Macromolecules* **2014**, *47*, 5542.

[51] N. Toshikj, J.-J. Robin, S. Blanquer, *Eur. Polym. J.* **2020**, *127*, 109599.

[52] K. Philipps, T. Junkers, J. J. Michels, *Polym. Chem.* **2021**, *12*, 2522.

[53] I. Van Der Meulen, M. De Geus, H. Antheunis, R. Deumens, E. A. J. Joosten, C. E. Koning, A. Heise, *Biomacromolecules* **2008**, *9*, 3404.

[54] H. Urayama, S.-I. Moon, Y. Kimura, *Macromol. Mater. Eng.* **2003**, *288*, 137.

[55] Y. Wang, X. Leng, Z. Wei, Y. Zhao, L. Zheng, Y. Li, *J. Mater. Sci.* **2020**, *55*, 9129.

[56] Z. Wei, R. Che, S. Shao, Y. Wang, X. Leng, Y. Li, *Polym. Test.* **2020**, *83*, 106348.

[57] Z. Jing, X. Shi, G. Zhang, *Polym. Int.* **2017**, *66*, 1487.

[58] M. L. Focarete, M. Scandola, A. Kumar, R. A. Gross, *J. Polym. Sci., Part B: Polym. Phys.* **2001**, *39*, 1721.

[59] R. Auras, H. Tsuji, L.-T. Lim, S. E. M. Selke, *Poly(Lactic Acid): Synthesis, Structures, Properties, Processing and Applications*, 1st ed., Wiley, New York **2010**.

[60] B. A. G. Schrauwen, R. P. M. Janssen, L. E. Govaert, H. E. H. Meijer, *Macromolecules* **2004**, *37*, 6069.

[61] A. I. Leonov, *Int. J. Solids Struct.* **2002**, *39*, 5913.

[62] Z. Bartczak, A. Galeski, *Macromol. Symp.* **2010**, *294*, 67.

[63] J. Petermann, H. Ebener, *Polymer* **1996**, *38*, 837.

[64] A. Pawlak, A. Galeski, A. Rozanski, *Prog. Polym. Sci.* **2014**, *39*, 921.

[65] P. Wang, I. M. Hutchings, S. J. Duncan, L. Jenkins, E. Woo, *J. Mater. Sci.* **2006**, *41*, 4847.

[66] P. I. Vincent, *Polymer* **1960**, *1*, 7.

[67] Z. Kulinski, E. Piorkowska, K. Gadzinowska, M. Stasiak, *Biomacromolecules* **2006**, *7*, 2128.

[68] W. Pivsa-Art, K. Fujii, K. Nomura, Y. Aso, H. Ohara, H. Yamane, *J. Appl. Polym. Sci.* **2016**, *133*, 8.

[69] T. I. Croll, A. J. O'connor, G. W. Stevens, J. J. Cooper-White, *Biomacromolecules* **2004**, *5*, 463.

[70] S. Chen, L. Li, C. Zhao, J. Zheng, *Polymer* **2010**, *51*, 5283.

[71] P. A. Tran, T. J. Webster, *Int. J. Nanomed.* **2013**, *8*, 2001.

[72] X. Niu, Y. Luo, Y. Li, C. Fu, J. Chen, Y. Wang, *J. Biomed. Mater. Res., Part A* **2008**, *84A*, 908.

[73] J. Jinyoon, *Biomaterials* **2004**, *25*, 5613.

[74] G. Narayanan, V. N. Vernekar, E. L. Kuyinu, C. T. Laurencin, *Adv. Drug Delivery Rev.* **2016**, *107*, 247.

[75] S. Wang, W. Cui, J. Bei, *Anal. Bioanal. Chem.* **2005**, *381*, 547.

[76] Z. Zhang, Y. Lai, L. Yu, J. Ding, *Biomaterials* **2010**, *31*, 7873.

[77] K. M. Hennessy, B. E. Pollot, W. C. Clem, M. C. Phipps, A. A. Sawyer, B. K. Culpepper, S. L. Bellis, *Biomaterials* **2009**, *30*, 1898.

[78] X. He, J. Ma, E. Jabbari, *Langmuir* **2008**, *24*, 12508.

2300066 (14 of 14)